Analyst

PAPER

View Article Online
View Journal

Cite this: DOI: 10.1039/c4an02056a

Real-time monitoring of H_2O_2 release from single cells using nanoporous gold microelectrodes decorated with platinum nanoparticles†

Chong Xiao, Yan-Ling Liu, Jia-Quan Xu, Song-Wei Lv, Shan Guo and Wei-Hua Huang*

Received 8th November 2014,
Accepted 10th January 2015

DOI: 10.1039/c4an02056a

www.rsc.org/analyst

Here, we report a self-supported nanoporous gold microelectrode decorated with well-dispersed and tiny platinum nanoparticles as an electrochemical nonenzymatic hydrogen peroxide biosensor. Nanoporous gold was fabricated by electrochemical alloying/dealloying and then small-sized platinum nanoparticles were electrodeposited uniformly on them. This novel hybrid nanostructure endows the sensor with high sensitivity and selectivity towards the reduction of hydrogen peroxide with a low detection limit of 0.3 nM. The sensor has been successfully applied for the measurement of H_2O_2 release from a single isolated human breast cancer cell, demonstrating its great potential for further physiological and pathological applications.

1. Introduction

Hydrogen peroxide (H_2O_2), as a signaling molecule, plays critical roles in regulating diverse biological processes,[1] such as DNA repair,[2] oxidative activity,[3] host defense,[4] and apoptosis.[5] Thus, the rapid, accurate and sensitive determination of H_2O_2 is of great importance to study its physiological and pathological functions. Techniques available mainly include titrimetry,[6] spectrophotometry,[7] chemiluminescence,[8] electrochemistry,[9–11] fluorescence[12] and electron spin resonance.[13] Among these techniques, an electrochemical sensor, especially the one based on microelectrodes, is distinguished for its unique characteristics of high sensitivity, fast response and easy miniaturization, which enable it to be a powerful tool for real-time quantitative detection in biological systems.[14,15]

A number of electrochemical enzyme sensors have been developed to improve the electrocatalysis for detecting H_2O_2.[9,16,17] Nevertheless, the biocatalytic activities of enzymes are easily affected by the environment (such as temperature and pH) and the immobilization procedure, and the detection limits are usually restricted within the sub-micromolar regime. Subsequently, the advent of nanomaterials, including metal nanoparticles,[18] carbon nanomaterials[19,20] and metallic oxide nanostructures,[21] has brought H_2O_2 sensing to a non-enzymatic era, and tremendous sensors with high sensitivity and good stability have been constructed. Many biosensors with good responsiveness have been developed and used for the measurement of H_2O_2 released from the populations of living cells or the concentrated cytoplasm after lysis.[22–26] Notably, platinum (Pt) nanomaterials act as an excellent electrochemical catalyst to H_2O_2, benefiting from its function in promoting the electron transfer and reducing the over-potential.[11] In the field of single cell analysis using Pt nanomaterials as a catalyst, a pioneering work of H_2O_2 monitoring from a single isolated cell was reported by Amatore's group to study oxidative stress using a platinized carbon-fiber microelectrode.[14,27] Moreover, our group developed a uniform Pt nanoparticles (NPs) modified carbon fiber microelectrode and monitored the oxidative burst from individual living plant protoplasts.[28]

To increase Pt loading and obtain uniformly small-sized NPs, carbon nanotubes,[29] graphene,[30] nanowires[31] and polymers[32] have been explored as templates to homogeneously disperse PtNPs on the electrode surface. However, the area enhancement is limited because it focuses only on the utilization of the geometric surface. Furthermore, the composite nanostructures usually need to be further modified on the surface of the electrodes. The assembled electrochemical sensor usually exhibits an undesirably low electronic conductance as a consequence of exceptionally low electron transport in the nanomaterials as well as the high contact resistances between the current collector and electrodes.[33–35] To date, there are few reports concerning the three dimensional (3D) and conductive substrate to support nanoparticles for the construction of sensors.

Key Laboratory of Analytical Chemistry for Biology and Medicine (Ministry of Education), College of Chemistry and Molecular Sciences, Wuhan University, Wuhan, 430072, China. E-mail: whhuang@whu.edu.cn; Fax: +86-27-68754067; Tel: +86-27-68752149

†Electronic supplementary information (ESI) available: Fig. S1–S6. See DOI: 10.1039/c4an02056a

Herein, we report a self-supported microelectrode with a seamless solid/nanoporous gold/PtNPs hybrid (NPG/PtNPs) nanostructure to develop a H_2O_2 biosensor with high sensitivity, as well as high spatial and temporal resolution. Gold microwire structured with bicontinuous nanoporosity, which was fabricated by electrochemical alloying/dealloying in an electrolyte composed of $ZnCl_2$ and benzyl alcohol (BA),[35–38] was adopted as self-supported microelectrodes to adequately make use of the surface area of 3D nanomaterials. Then, small-sized and uniform PtNPs were electrodeposited on the ligament of mercaptoethylamine-pretreated NPG. The as-prepared nanostructure exhibited remarkable catalytic activity toward the electrochemical reduction of H_2O_2 with a sub-nanomolar sensitivity. The excellent performance results from the elaborate design that NPG provides the interconnected nanoporous channels to facilitate the transport of H_2O_2 and electron, and the continuous skeletons offer large area for PtNP loading and avoid particle aggregation. Moreover, the direct generation of a 3D bicontinuous NPG layer on the gold microwires could minimize the contact resistances among the current collector of the solid gold wire, nanoporous gold skeleton and PtNPs. The sensor was further successfully used for the real-time monitoring of H_2O_2 released from single human breast cancer cells.

2. Experimental

2.1 Reagents

Gold wire (25 μm in diameter, purity >99.99%) was purchased from Goodfellow Cambridge Limited. Phorbol myristate acetate (PMA), chloroplatinic acid hexahydrate ($H_2PtCl_6{\cdot}6H_2O$), catalase, 3-morpholinosydnonimine (SIN-1) and KO_2 were purchased from Sigma-Aldrich. Cysteamine hydrochloride ($C_2H_7NS{\cdot}HCl$) was obtained from Alfa Aesar. Hydrogen peroxide (H_2O_2, 30%), zinc chloride ($ZnCl_2$), concentrated H_2SO_4, and benzyl alcohol (BA) were of analytical grade and obtained from Sinopharm Chemical Reagent Co., Ltd. Solutions with desired concentration of H_2O_2 were freshly diluted with deoxygenized 0.1 M phosphate buffer solution (PBS, pH 7.4) from the 30% solution. In the selectivity test, superoxide anion ($O_2^{\bullet-}$) was derived from dissolved KO_2 in the DMSO solution, $ONOO^-$ was generated by dissolving 3-morpholinosydnonimine (SIN-1) into PBS (pH 7.4), and hypochlorite anion (ClO^-) was generated by NaClO. For all the experiments, deionized water (18.0 MΩ) purified using a Millipore system was used.

2.2 Apparatus

All the electrochemical measurements were carried out on a CHI 660A electrochemical workstation (CHI Instruments, Shanghai, China) at room temperature. A three-electrode system was used in the experiment including a NPG/PtNPs working electrode (WE), Ag/AgCl reference electrode and Pt counter electrode. Moreover, a two-electrode system was employed for the cell experiments. SEM images were obtained on a field-emission scanning electron microscope (Zeiss SIGMA). The TEM images were acquired on a JEM-2100 transmission electron microscope. In the cell experiment, two micromanipulators (TransferMan NK2, Eppendorf, Hamburg, Germany) were used for precise positioning. A TS2-60 multi Syringe pump (LongerPump Co., Ltd) was used in conjunction with one of the micromanipulators for stimulant injection. An inverted fluorescent microscope (Axiovert 200M, Zeiss, Germany) was utilized for observation.

2.3 Fabrication of NPG microelectrode

In brief, the gold microwire (Scheme 1A) was cut into 0.3 cm length, and then was connected to a copper wire *via* conductive glue and the joint was wrapped with tape, followed by sealing with polydimethylsiloxane. Before alloying/dealloying, the gold wires were ultrasonically degreased in acetone, ethanol and distilled water for a few minutes. The electrochemical alloying/dealloying process was performed in a three-electrode electrochemical cell, in which the Zn plate and Zn wire were used as the auxiliary electrode and the reference electrode, respectively, in a BA electrolyte containing 1.5 M $ZnCl_2$. A 3D bicontinuous nanoporous layer was generated on polished gold wires after 5 cycles in the potential range from −0.72 to 1.88 V at 120 °C with a scan rate of 10 mV s^{-1} (Scheme 1B).[35–38] Before and after etching, the electrode was cleaned by cyclic voltammetry in 0.5 M H_2SO_4 from 0.4 V to 1.5 V until a reproducible scan was obtained. The NPG electrode was thoroughly rinsed with deionized water and dried under flowing nitrogen.

2.4 Electrodeposition of PtNPs into NPG

To enhance the signal/noise ratio of the NPG for amperometric detection on single cells, we obtained a NPG microdisk electrode by selectively insulating the electrode with photoresist that has been described in our previous work.[39] Briefly, the microelectrode was immersed into an AZ4620 photoresist for 5 minutes, followed by heating in an oven at 75 °C for 4 minutes and 105 °C for 6 minutes. The above process was repeated again to ensure that all the active area was insulated with photoresist. The precise removal of photoresist covered on the tip of the electrode was performed in H_2SO_4–H_2O_2 (v/v = 7 : 3) solution with the aid of a micromanipulator, revealing the exposed tip of 1–2 μm in length (Scheme 1C). Before the electrodeposition of PtNPs, the clean NPG microdisk electrode was immersed in 0.1 mM mercaptoethylamine or cyste-

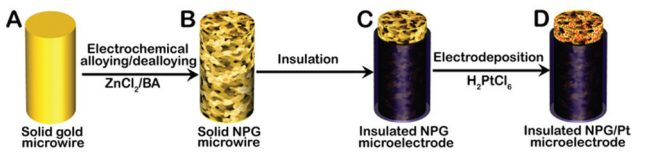

Scheme 1 The fabrication of hybrid microelectrodes. (A) Solid gold microwire. (B) 3D bicontinuous NPG layer is formed directly on the solid gold microwire by electrochemical alloying/dealloying in a mixed electrolyte of BA and $ZnCl_2$. (C) The insulated NPG microelectrode. (D) PtNPs are decorated on the nanopore channels of the NPG microelectrode by electrodeposition in a mixed solution containing H_2PtCl_6.

amine (Cys) solution for 4 h at room temperature to form a NPG-Cys self-assembly microelectrode. At the end of this period, the microdisk electrode (NPG-Cys) was rinsed with double distilled water to wash-off the physically adsorbed mercaptoethylamine. After allowing it to stand in 0.5 mM H_2PtCl_6 solution for 2 hours, the NPG-Cys microelectrode acted as the WE to electrodeposit PtNPs for 100 s at the potential of −0.6 V (*vs.* Ag/AgCl) with 0.2 M Na_2SO_4 as the supporting electrolyte (Scheme 1D).

2.5 Single cell experiments

Human breast cancer cells MCF-7 were obtained from China Center for Type Culture Collection. The cells were maintained in Dulbecco's modified Eagle's medium supplemented with 10% fetal bovine serum, 1% double-antibody and incubated at 37 °C in a humidified incubator (5% CO_2–95% air). Prior to the cell experiments, the cells were transferred on a slide and incubated for 24 h. Single cell experiments were performed at room temperature on the stage of an inverted fluorescent microscope placed in a copper shield. H_2O_2 released from single cells was detected in real-time using the CHI 660A workstation at a constant potential of −0.2 V. For the detection of extracellular H_2O_2 released from MCF-7, the cells were stimulated with 100 ng ml^{-1} PMA.[40,41] In control experiment, the cells were stimulated by PBS, or the cells were incubated with catalase for 10 min before stimulation by PMA.

3. Results and discussion

3.1 Fabrication and characterization of NPG/PtNPs

The fabrication process of the NPG/PtNPs electrode is illustrated in Scheme 1. First, a 3D bicontinuous NPG layer was directly formed on the solid gold microwire by *in situ* electrochemical alloying/dealloying in a mixed electrolyte of $ZnCl_2$ and BA. Fig. 1A shows the representative top-view FESEM and TEM images of the NPG. A uniform and 3D bicontinuous porous structure can be clearly observed. Both gold skeletons and the pores are spatially interconnected, and the entire surfaces of NPG skeletons are smooth with a clear surface contour. Roughness factor is defined as the ratio between the real surface area and the geometrical area of the electrode. In the case of the gold electrode, the charge associated with the reduction of gold oxide was proportional to the real active surface area of the gold electrode.[42] Cyclic voltammograms (CV) in 0.5 M H_2SO_4 solution was employed to evaluate the electrochemically active surface area of the initial gold microwire and NPG (Fig. 1B), and the roughness factors of three individual NPG microelectrodes were estimated to be 86, 110 and 115, respectively.

The NPG/PtNPs hybrid microelectrodes were synthesized by the electrodeposition with H_2PtCl_6 as the precursor. To obtain well-distributed PtNPs, here we modified the NPG microelectrode with a monolayer of mercaptoethylamine through an Au–S bond before electrodeposition, considering that the positively charged $-NH_2$ might promote the pre-absorption of $PtCl_6^{2-}$ on the skeleton surface. The following results also confirmed that the mercaptoethylamine layer on NPG could not only dramatically improve the Pt electrodeposition efficiency but also benefit the uniform dispersion of PtNPs, in which the loading amount and morphology of PtNPs can be tailored by the concentration of H_2PtCl_6 (Fig. S1†), the applied potential (Fig. S2†) and the electrodeposition time (Fig. S3†). As illustrated in Fig. S2,† the generated PtNPs become more dispersed when the potential is more negative. Moreover, at a constant potential of −0.6 V, the loading amount of PtNPs increases with the increasing concentration of H_2PtCl_6. In 0.1 mM H_2PtCl_6, only a few PtNPs can be observed from the FESEM image; however, when the concentration is increased to 1 mM, PtNPs start to aggregate, which leads to the blocking of nanopores on the gold skeleton. In the mixed solution containing 0.5 mM H_2PtCl_6, the small-sized PtNPs uniformly and directly grow into nanopores along the gold ligaments of the NPG at a constant applied potential of −0.6 V for 100 s. In contrast, under the same conditions, PtNPs seriously aggregate on the surface of the solid gold wire electrode (Fig. S3D†). In Fig. 2A, the FESEM image reveals that there are abundant tiny PtNPs densely covered on the surface of the 3D bicontinuous NPG, forming a rough gold skeleton. Furthermore, from the TEM image (Fig. 2B), we can clearly see that PtNPs are well-dispersed with a diameter of about 5–10 nm. The results indicate that the NPG used here as a supporting matrix could efficiently disperse PtNPs, preventing them from serious aggregation, and thus preserving the high catalytic performance of PtNPs. The unique bicontinuous structure of NPG and well-dispersed PtNPs will contribute to a large specific surface area of the

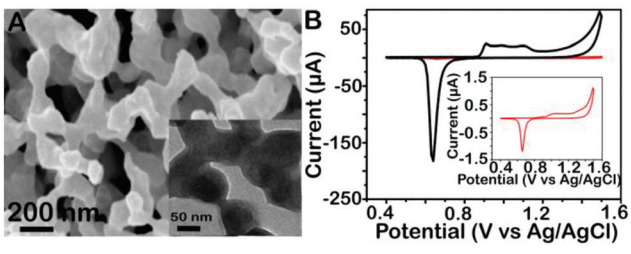

Fig. 1 (A) Top-view FESEM image of NPG, and the inset is the TEM image of the as-prepared NPG. (B) CV curves of the gold microwire (red line) and NPG (black line) electrodes in 0.5 M H_2SO_4 solution at a scan rate of 100 mV s^{-1}. Inset: an enlarged curve for the solid gold microwire.

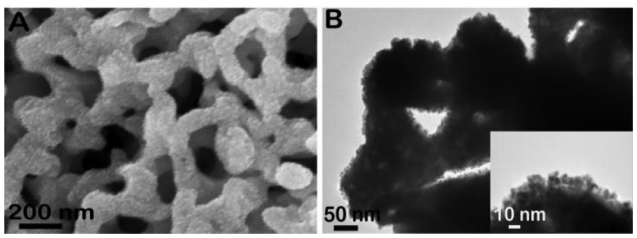

Fig. 2 (A) Top-view FESEM image of the as-prepared NPG/PtNPs hybrid. (B) TEM image of the as-prepared NPG/PtNPs hybrid, and the inset is magnified TEM image of NPG/PtNPs hybrid.

electrode–electrolyte interface, facilitating the enhanced electrocatalysis of the NPG/PtNPs hybrid towards H_2O_2.

3.2 Electrochemical characterization of NPG/PtNPs

To eliminate the individual difference of electrochemical behavior between different electrodes, the comparison between the NPG electrode and the NPG/PtNPs electrode was based on the same gold electrode. Recent studies have found that the performance of the H_2O_2 sensor strongly depends on the size, distribution and loading amount of PtNPs on the electrode. The uniformly small-sized PtNPs could provide large number of active sites for obtaining contact with H_2O_2 for the electrocatalytic process.[29,43,44] Positive shift in the reduction peak potential and increase in the peak current were also obtained while increasing the loading of PtNPs on the electrode surface (Fig. S4†). Under optimized conditions, it is clearly indicated that the reduction current of the NPG/PtNPs microelectrode to H_2O_2 is considerably higher than that on the NPG microelectrode (Fig. 3A). The onset reduction potential of the NPG/PtNPs microelectrode towards H_2O_2 was about −0.05 V, which is about 200 mV positively shifted compared with that of the bare NPG electrode, and a reductive peak appeared at around −0.2 V. As a comparison, there is no apparent reduction current without H_2O_2, further confirming that the current is generated *via* the catalytic reduction of H_2O_2. The positively-shifted reduction potential and the significantly enhanced peak current clearly demonstrate that the NPG/PtNPs microelectrode has much higher catalysis towards the reduction of H_2O_2 than the bare NPG microelectrode. This remarkable catalytic activity toward the electrochemical reduction of H_2O_2 could be ascribed to the following factors.

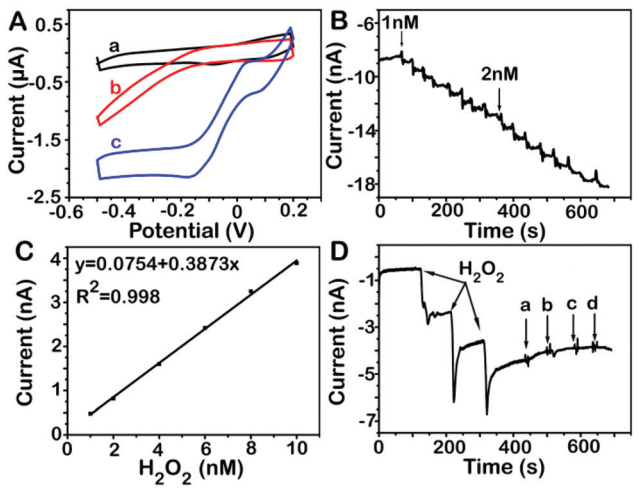

Fig. 3 (A) CV curves of NPG (b) and NPG/PtNPs (a, c) microelectrodes in deoxygenized PBS with 2 mM H_2O_2 (b, c) or without H_2O_2 (a) at a scan rate of 50 mV s^{-1}. (B) Amperometric responses of insulated NPG/PtNPs microelectrodes to the successive addition of H_2O_2 in 0.1 M PBS at an applied potential of −0.2 V. (C) Calibration curve of the insulated NPG/PtNPs microelectrode for the increasing concentrations of H_2O_2. (D) Amperometric responses of insulated NPG/PtNPs microelectrodes to the additions of 5 μM H_2O_2, NO_2^- (a), ClO^- (b), $ONOO^-$ (c) and $O_2^{\bullet-}$ (d).

First, small-sized PtNPs intrinsically possess an excellent electrochemical catalysis to H_2O_2. Second, a mercaptoethylamine modified 3D conductive NPG substrate, which possesses much higher roughness and better electron transport, was adopted as self-supported microelectrodes to support PtNPs. The structure could disperse and increase the load amount of small-sized PtNPs to provide a large number of active sites, preventing them from aggregation. Third, synergistic electrocatalytic activity between the gold skeleton and PtNPs also plays an important role.

To further enhance the signal/noise ratio of the NPG/PtNPs microelectrode for amperometric detection and the single cell experiments, the NPG/PtNPs microelectrode was insulated by photoresist and the tip was then selectively revealed to get a microdisk electrode (Scheme 1). Fig. 3B and S5† display steady-state amperometric responses of the NPG/PtNPs and solid gold/PtNPs microdisk electrodes with the same geometric size to different concentrations of H_2O_2 at a potential of −0.2 V. With the additions of low concentrations of H_2O_2 (1 nM, 2 nM and 5 nM), there were no amperometric responses on the solid gold/PtNPs microdisk electrode, while the NPG/PtNPs microelectrode responded rapidly to achieve the maximum steady-state current within 5 s. An obvious step increase of the current could be observed when the concentration of H_2O_2 was as low as 1 nM. The detection limit of the NPG/PtNPs microdisk electrode was calculated to be about 0.3 nM (S/N = 3), being the lowest compared to those reported previously. The low detection limit of the sensor combined with its ultra-small geometric size facilitate the NPG/PtNPs microdisk electrode to monitor H_2O_2 information on the single cell level or other biological microenvironments in real-time.

The selectivity of NPG/PtNPs toward H_2O_2 was further studied by an investigation in the presence of interfering species. In this work, the applied potential (−0.2 V) could minimize the responses of common interference species. The response of common coexisting reactive oxygen species (ROS) and compounds in the biological system such as $O_2^{\bullet-}$, $ONOO^-$, ClO^-, NO_2^-, AA and UA was recorded at the NPG/PtNPs microdisk electrode. Fig. 3D and S6† show that the response current of the sensor greatly changed after the addition of H_2O_2, while nearly no current change could be observed with the addition of common ROS and compounds. This suggests that the biosensor performs with high selectivity toward H_2O_2 over these biologically relevant ROS and compounds.

3.3 Monitoring of extracellular H_2O_2 released from single cells

It is of great significance to sensitively detect H_2O_2 owing to its diverse biological functions. Here, we used the constructed NPG/PtNPs microdisk electrode to monitor extracellular H_2O_2 released from single isolated MCF-7 cells. Prior to the measurements, a slide with cells on it was placed in a chamber, which served as an electrolytic cell. Under the microscope, we placed the tip of the sensor 1 μm away from the surface of a single MCF-7 cell by a micromanipulator. In the

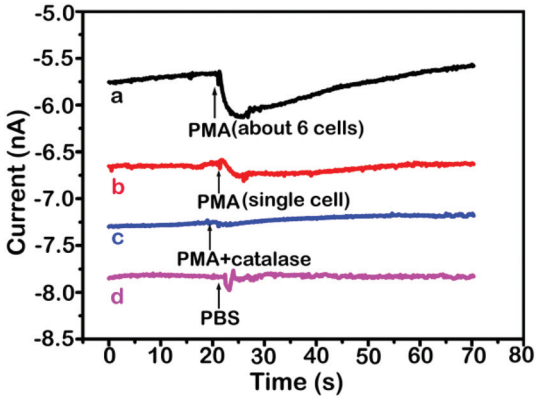

Fig. 4 Amperometric measurement of H_2O_2 released from MCF-7 cells at insulated NPG/PtNPs microelectrodes. Typical responses of H_2O_2 release from about 6 MCF-7 cells (a) and a single MCF-7 cell (b) stimulated with PMA. Typical response of H_2O_2 release from MCF-7 cells stimulated with PMA after the incubation of the cells with catalase (c). Typical response of H_2O_2 release from MCF-7 cells stimulated with PBS (d).

opposite direction, a microcapillary filled with stimulus was positioned by another micromanipulator (this micromanipulator was connected with the pump for injection) to the place where the distance between the cell and the outlet of the microcapillary was about 70 μm. The H_2O_2 release was triggered by stimulation with 100 ng mL^{-1} phorbol myristate acetate (PMA) for 5 s, a compound that can induce H_2O_2 generation in cells.[40,41] From Fig. 4, we can see that upon the injection of PMA, a sharp increase in current could be achieved within 5 s. Subsequently, the current decreased to the background level within 40 s, indicating that H_2O_2 is either consumed or diffused away from the electrode surface. Control experiments were carried out to confirm that the changes in the measured current observed were due to the electroreduction of H_2O_2 released from MCF-7 cells. In control experiment, the cells were stimulated by phosphate buffer, or the cells were incubated with catalase (with a final concentration of 100 U ml^{-1}), a H_2O_2 scavenger, for 10 min before it was stimulated by PMA. No current increase was observed if catalase was added into PBS solution (Fig. 4). This indicated that most of the H_2O_2 molecule released from cells had been consumed by catalase. Similarly, no increase in current was observed when the sham stimulus phosphate buffer was injected. The overall experimental results demonstrated the powerful ability of the NPG/PtNPs microdisk electrode to detect H_2O_2 released from single MCF-7 cells with high sensitivity.

4. Conclusions

In summary, we have constructed a highly sensitive and selective H_2O_2 microsensor by the electrodeposition of small-sized and well-dispersed Pt nanoparticles on self-supported bicontinuous nanoporous gold microelectrodes. The microsensor displayed excellent electrocatalysis for the reduction of H_2O_2 and has a low detection limit of 0.3 nM. Owing to its ultra-small geometric size and high sensitivity, the real-time monitoring of H_2O_2 release from a single MCF-7 cell was achieved using this microsensor. The excellent catalytic performance and its capacity to detect H_2O_2 on a single cell level make this biosensor to be a potentially useful tool for further physiological and pathological applications.

Acknowledgements

This work was supported by the National Science Foundation of China (nos. 21375099, 91017013), Specialized Research Fund for the Doctoral Program of Higher Education (20120141110031) and the Fundamental Research Funds for the Central Universities (2042014kf0192).

References

1 T. Finkel and N. J. Holbrook, *Nature*, 2000, **408**, 239–247.
2 M. B. Yaffe and L. C. Cantley, *Nature*, 1999, **402**, 30–31.
3 J. D. Scott and T. Pawson, *Science*, 2009, **326**, 1220–1224.
4 D. Trachootham, J. Alexandre and P. Huang, *Nat. Rev. Drug Discovery*, 2009, **8**, 579–591.
5 M. C. Y. Chang, A. Pralle, E. Y. Isacoff and C. J. Chang, *J. Am. Chem. Soc.*, 2004, **126**, 15392–15393.
6 S. Chen, R. Yuan, Y. Chai, L. Zhang, N. Wang and X. Li, *Biosens. Bioelectron.*, 2007, **22**, 1268–1274.
7 R. C. Matos, E. O. Coelho, C. F. Souza, F. A. Guedes and M. A. Matos, *Talanta*, 2006, **69**, 1208–1214.
8 Z. Wang, F. Liu, X. Teng, C. Zhao and C. Lu, *Analyst*, 2011, **136**, 4986–4990.
9 W. Chen, S. Cai, Q. Q. Ren, W. Wen and Y. D. Zhao, *Analyst*, 2012, **137**, 49–58.
10 M. Roushani, E. Karami, A. Salimi and R. Sahraei, *Electrochim. Acta*, 2013, **113**, 134–140.
11 X. Y. Li, X. H. Liu, W. W. Wang, L. Li and X. Q. Lu, *Biosens. Bioelectron.*, 2014, **59**, 221–226.
12 B. C. Dickinson, C. Huynh and C. J. Chang, *J. Am. Chem. Soc.*, 2010, **132**, 5906–5915.
13 G. Bartosz, *Clin. Chim. Acta*, 2006, **368**, 53–76.
14 C. Amatore, S. Arbault, M. Guille and F. Lemaître, *Chem. Rev.*, 2008, **108**, 2585–2621.
15 W. B. Nuwall and W. G. Ktihr, *Electroanalysis*, 1997, **9**, 102–109.
16 J. B. Jia, B. Q. Wang, A. G. Wu, G. J. Cheng, Z. Li and S. J. Dong, *Anal. Chem.*, 2002, **74**, 2217–2223.
17 Y. P. Luo, H. Q. Liu, Q. Rui and Y. Tian, *Anal. Chem.*, 2009, **81**, 3035–3041.
18 W. Lu, F. Liao, Y. Luo, G. Chang and X. Sun, *Electrochim. Acta*, 2011, **56**, 2295–2298.
19 X. Cao, Z. Zeng, W. Shi, P. Yep, Q. Yan and H. Zhang, *Small*, 2013, **9**, 1703–1707.
20 J. Tkac and T. Ruzgas, *Electrochem. Commun.*, 2006, **8**, 899–903.

21 B. Sÿljukic, C. E. Banks and R. G. Compton, *Nano Lett.*, 2006, **6**, 1556–1558.
22 C. X. Guo, X. T. Zheng, Z. S. Lu, X. W. Lou and C. M. Li, *Adv. Mater.*, 2010, **22**, 5164–5167.
23 P. Wu, Z. W. Cai, Y. Gao, H. Zhang and C. X. Cai, *Chem. Commun.*, 2011, **47**, 11327–11329.
24 T. Wang, H. Zhu, J. Zhuo, Z. Zhu, P. Papakonstantinou, G. Lubarsky, J. Lin and M. Li, *Anal. Chem.*, 2013, **85**, 10289–10295.
25 X. Sun, S. Guo, Y. Liu and S. Sun, *Nano Lett.*, 2012, **12**, 4859–4863.
26 Y. Zhang, C. Wu, X. Zhou, X. Wu, Y. Yang, H. Wu, S. Guo and J. Zhang, *Nanoscale*, 2013, **5**, 1816–1819.
27 S. Arbault, P. Pantano, J. A. Jankowski, M. Vuillaume and C. Amatore, *Anal. Chem.*, 1995, **67**, 3382–3390.
28 F. Ai, H. Chen, S. H. Zhang, S. Y. Liu, F. Wei, X. Y. Dong, J. K. Cheng and W. H. Huang, *Anal. Chem.*, 2009, **81**, 8453–8458.
29 X. Li, X. Liu, W. Wang, L. Li and X. Lu, *Biosens. Bioelectron.*, 2014, **59**, 221–226.
30 F. Xu, Y. Sun, Y. Zhang, Y. Shi, Z. Wen and Z. Li, *Electrochem. Commun.*, 2011, **13**, 1131–1134.
31 M. Sudan Saha, R. Li, M. Cai and X. Sun, *Electrochem. Solid-State Lett.*, 2007, **10**, B130–B133.
32 C. Li, J. Hu, T. Liu and S. Liu, *Macromolecules*, 2011, **44**, 429–431.
33 S. R. Gowda, A. L. M. Reddy, X. B. Zhan, H. R. Jafry and P. M. Ajayan, *Nano Lett.*, 2012, **12**, 1198–1202.
34 F. Léonard and A. A. Talin, *Nat. Nanotechnol.*, 2011, **6**, 773–783.
35 X. Y. Lang, H. Y. Fu, C. Hou, G. F. Han, P. Yang, Y. B. Liu and Q. Jiang, *Nat. Commun.*, 2013, **4**, 2169, DOI: 10.1038/ncomms3169.
36 C. F. Yu, F. L. Jia, Z. H. Ai and L. Z. Zhang, *Chem. Mater.*, 2007, **19**, 6065–6067.
37 J. H. Jiang and X. Y. Wang, *Electrochem. Commun.*, 2012, **20**, 157–159.
38 J. H. Jiang and X. Y. Wang, *ECS Electrochem. Lett.*, 2012, **1**(5), H21–H23.
39 J. T. Liu, L. S. Hu, Y. L. Liu, R. S. Chen, Z. Cheng, S. J. Chen, C. Amatore, W. H. Huang and K. F. Huo, *Angew. Chem., Int. Ed.*, 2014, **53**, 2643–2647.
40 A. W. Griffith and J. M. Cooper, *Anal. Chem.*, 1998, **70**, 2607–2612.
41 P. Wu, Y. Qian, P. Du, H. Zhang and C. Cai, *J. Mater. Chem.*, 2012, **22**, 6402–6412.
42 S. Trasatti and O. A. Petrii, *Pure Appl. Chem.*, 1991, **63**, 711–734.
43 Z. M. Peng and H. Yang, *Nano Today*, 2009, **4**, 143–164.
44 Z. Chen, M. Waje, W. Li and Y. S. Yan, *Angew. Chem., Int. Ed.*, 2007, **46**, 4060–4063.